The Detectability Limit of Organic Molecules within Mars South Polar Laboratory Analogues

Jacqueline D Campbell, B Schmitt, O. Brissaud, J.-P. Muller

The Detectability Limit of Organic Molecules within Mars South Polar Laboratory Analogues

J. D. Campbell [1,2], B. Schmitt [3], O. Brissaud [3], J-P. Muller [1]

[1] Imaging Group, Mullard Space Science Laboratory, Department of Space and Climate Physics, University College London (UCL), Holmbury St. Mary, RH5 6NT, UK

[2] now at Dept. of Earth Sciences, University of Oxford, OX1 3AN, UK

[3] Université Grenoble Alpes, CNRS, Institut de Planétologie et d'Astrophysique de Grenoble, France

Corresponding author: Jacqueline D. Campbell (jacqueline.campbell@earth.ox.ac.uk)

Key Points:

- A new spectrum diagnostic of Polycyclic Aromatic Hydrocarbons (PAHs) pertinent to Mars has been produced
- The detectability limit of PAHs in Mars South Pole analogues has been established
- The evolution of the spectra of PAHs in Mars South Pole analogues as ice sublimates under emulated Martian conditions has been recorded

Abstract

A series of laboratory experiments was carried out in order to generate a diagnostic spectrum for Polycyclic Aromatic Hydrocarbons (PAHs) of astrobiological interest in the context of the Martian South Polar Residual Cap (SPRC), to establish PAH spectral features more easily detectable in CO_2 ice (mixed with small amounts of H_2O ice) than the previously reported absorption feature at 3.29 μm in order to constrain their detectability limit. There is currently no existing literature on PAH detection within SPRC features, making this work novel and impactful given the recent discovery of a possible subglacial lake beneath the Martian South Pole. Although they have been detected in Martian meteorites, PAHs have not been detected yet on Mars, possibly due to the deleterious effects of ultraviolet radiation on the surface of the planet. SPRC features may provide protection to fragile molecules, and this work seeks to provide laboratory data to improve interpretation of orbital remote sensing spectroscopic imaging data. We also ascertain the effect of CO_2 ice sublimation on organic spectra, as well as provide PAH reference spectra in mixtures relevant to Mars. A detectability limit of ~0.04% has been recorded for observing PAHs in CO_2 ice using laboratory instrument parameters emulating those of the Compact Reconnaissance Imaging Spectrometer for Mars (CRISM), with new spectral slope features revealed between 0.7 and 1.1 μm, and absorption features at 1.14 and, most sensitively, at 1.685 μm. Mars regolith analogue mixed with a concentration of 1.5% PAHs resulted in no discernible organic spectral features. These detectability limits measured in the laboratory are discussed and extrapolated to the effective conditions on the Mars South Polar Cap in terms of dust and water ice abundance and CO_2 ice grain size for both the main perennial cap and the H_2O ice-dust sublimation lag deposit.

Plain Language Summary

Carbon molecule chains, or organics, are considered important in the search for life, as all life that we know of on Earth is made from carbon. A particular type of organic, PAHs, that are really common on Earth and throughout space, have never been found on Mars and it is likely they are broken down too quickly on the Martian surface by the Sun's radiation to be discovered using space satellites. However, some areas of Mars move and change, and expose dust. One such area is the Martian South Polar Cap. This study uses laboratory experiments to simulate expected conditions on the Mars South Pole, and mix PAHs with ices, then look at them using instruments similar to those on satellites orbiting Mars to find out how much PAH material would have to be in the ice to be able to detect it. These experiments allowed us to create a spectrum that can be used to help to identify different materials. We have found that you can observe features of PAHs at 1.685 and 1.14 μm in the spectra when there is 0.1% or more PAH in a carbon dioxide ice sample, but it was not possible to see 1.5% of PAH in a sample of dust similar to the dust on the surface of Mars.

1 Introduction

Our neighbouring planet, Mars, has increasingly been the target of scientific exploration and of particular interest are its geological history, current environmental conditions, and perhaps most importantly, its potential as a host for extraterrestrial life (Fairén et al., 2010). The polar caps of Mars have more recently emerged as an area of scientific interest due to their abundance of water ice and their dynamic nature, especially with the discovery of a possible stable body of liquid water beneath the Martian South Pole (Orosei et al., 2018). The Martian North and South Pole

have permanent ice caps that expand throughout their respective winters, and maintain residual caps in the summer. The North Polar Cap (NPC) is composed almost entirely of water ice, while the longer, colder winter in the higher altitude southern hemisphere means that the central part of the South Polar Cap (SPC) is covered by a permanent layer of CO_2 ice (Byrne, 2009), up to 10 metres thick, underlain, and surrounded by, water ice layers known as Polar Layered Deposits (PLD; Piqueux et al., 2008).

Seasonal cycles of sublimation and deposition of CO_2 ice on the SPC are responsible for the formation of 'Swiss Cheese Terrain' (SCT). This unique cryomorphology manifests as flat-topped mesas with flat floored, quasi-circular depressions that form patterns resembling Emmental Swiss Cheese (Malin et al., 2001). This terrain forms by preferential and progressive sublimation and erosion of the walls of the depressions, at a typical speed of 3 metres per Mars year. The reason these SCT sublimations features are of interest to this study is because of the exposure of dust previously shielded within the SPC (Jian et al., 2009). The exposed dust that has been concentrated by CO_2 ice sublimation may be a candidate site for the detection of a class of organic molecules, Polycyclic Aromatic Hydrocarbons (PAHs), that may have been protected from the Sun's radiation within the SPC. If PAH is dispersed in the ice instead of being associated with the dust, it will also be concentrated at the surface with the dust as the ice sublimates away leaving any particles behind.

Work was previously carried out in order to look for PAH signatures on the thin, dust-covered rims of SCT to no avail (Campbell et al., 2018) using the well-known PAH diagnostic absorption feature at 3.29 μm (Allamandola, 2011), but no signs of PAHs were found. However, this strong band is situated in the high wavelength wing of the very strong 3.1μm band of water ice and may thus be hidden in places where abundant water ice is present, such as on SPC margins (Douté et al. 2007) and rim scarps (Campbell at al., 2018). It may be also hidden by the wide hydration bands of minerals (adsorbed and structural water) that can extend up to 4 μm and may even be saturated in some cases.

The aims of the experiments carried out and reported here were to generate a diagnostic near-infrared spectrum for PAHs of astrobiological interest in the context of the Martian South Pole. We emulate the parameters of the CRISM instrument's Full Resolution Targeted (FRT) ~18 m/pixel mode to constrain the detectability limit of PAHs in CO_2 ice to establish the characteristics of PAH spectral features at wavelengths other than the absorption feature at 3.29 μm, where they might be easier to discern against the CO_2 and H_2O ice spectrum. In addition, we discuss how the detectability of these bands is affected by the presence of dust.

1.1 Polycyclic Aromatic Hydrocarbons

PAHs are a group of chemical compounds consisting of benzene rings of carbon with hydrogen. In its NPAH form, nitrogen can be substituted for carbon atoms in the aromatic ring (Tang, 2018). PAHs occur not only on Earth, but throughout the universe. They have been found to coalesce in space within dust clouds (Mulas et al., 2005), and are thought to account for up to 20% of total cosmic carbon (Allamandola, 2011).

PAHs frozen within ice particles in dense molecular clouds in space undergo processing by ultraviolet light and cosmic rays to produce more complex species (Dartnell et al., 2012). PAHs

can also arise and increase in abundance through the irradiation of complex polymeric organic material such as those found in carbonaceous meteorites (Thompson et al., 2020). A recent paper on the Mukundpura carbonaceous chondrite meteorite found in India measured 500ppm PAH (Kalpana et al., 2021). PAHs eventually rain down on primordial planets directly from planetary accretion discs, or are delivered on comets and meteorites (Allamandola, 2011). Therefore, PAHs should be present, or should have been present in the past, on all planetary bodies in the solar system (Dullemond et al., 2007). PAHs have been detected on the surfaces of Saturnian icy moons and comets (Cruikshank et al., 2008, 2014; Lopez-Puertas et al., 2013; Li, 2008) and have been measured in other carbonaceous chondrites meteorites at the level of a few ppm (Becker at al. 1997).

The delivery of complex organic compounds to planets via bolide impact is a very important concept in astrobiology, and could be instrumental in explaining abiogenesis (the origin of life). Carbon's propensity to catenate (form long chains), and the carbon-based nature of all life on Earth, means that the presence of carbon compounds is considered an essential component of any potentially habitable environment (Plaxco and Gross, 2011). PAHs are sought after on many solar system bodies in the search for the origin of life, but are conspicuously missing on Mars (Benner et al., 2000). The discovery of PAHs on Mars would tell us that these organics could survive in oxidizing environments receiving high levels of UV radiation, and may have accumulated in the past when Mars had warmer and wetter conditions favourable to the emergence of life.

1.2. PAHs on Mars

The detection of organics has been a primary objective of orbiters and landers since the Viking missions (Klein, 1978). Despite apparent negative results for the detection of extant life by the Viking landers in the 1970s, which searched for traces of biologically important compounds (Klein, 1978; Schuerger and Clark, 2008), perchlorates were discovered by the 2008 Phoenix lander (Hecht et al., 2009). More recently, organics were discovered by the Sample Analysis at Mars (SAM) instrument on NASA's 2012 rover mission, Mars Science Laboratory (Freissinet et al., 2015), known as "Curiosity". Perhaps of even more interest, is the re-analysis of the 1976 Viking Lander data by Navarro-Gonzalez et al. (2010) using modern laboratory techniques suggested that there were both perchlorates and organic carbon present at the Viking Lander sample sites, although they were not identified at the time. To date, no PAHs have been found on Mars, but concentrations of about 1ppm of PAH have been found in Martian meteorites with potential extraterrestrial origin (McKay et al. 1996, Becker at al., 1997; Botta and Bada, 2002). A study by Dartnell et al. (2012) found that PAHs might be afforded protection from the effects of UV radiation and oxidization within the subsurface of Mars, within rock, or in permanently shadowed areas. Ice can also provide a barrier to deep UV solar radiation (Vincent, 1998;

Cockell et al., 2000), resulting in partial shielding and allowing organic compounds to become more complex (Herbst and van Dishoek, 2009; Oberg et al., 2009).

2 Laboratory Analysis

2.1 Instruments

2.1.1. Laboratory Analysis

The site of the experiments was the Cold Surfaces Spectroscopy Facility (https://cold-spectro.sshade.eu) at the Institut de Planétologie et d'Astrophysique de Grenoble (IPAG) in France and has facilities for in-situ formation of ices, and cold rooms capable of keeping samples up to -40°C to allow stable thermal conditions during preparation of icy materials for experiments. This allows analysis of samples in the cryogenic CarboN-IR environmental cell, which can maintain cold temperatures and low gas pressures, using the SHINE (SpectropHotometer with variable INcidence and Emergence) instrument to record reflectance spectra in visible and near-mid infrared wavelengths.

2.1.2. Spectro-gonio radiometer

The SHINE spectro-gonio radiometer was developed at IPAG, and is designed to measure bidirectional reflectance and polarisation distribution functions of planetary material, enabling the production of accurate datasets to help describe surface composition, roughness and texture (Brissaud et al., 2004). In particular, the SHINE spectro-gonio radiometer is able to characterise the light scattering properties of snows of various grain-size, compactness and surface roughness at different stages of metamorphism. The instrument is able to measure from 0.35-4.80 μm, with spectral resolution of between 6-40 nm, dependent on wavelength (ibid).

SHINE can be used in conjunction with the CarboN-IR environmental cell to analyse materials at low temperatures.

2.1.3. CarboN-IR Environmental Cell

The CarboN-IR environmental cell system (https://cold-spectro.sshade.eu/carbo-nir-simulation-chamber) allows for the study of planetary material samples in stable conditions. It can cool the sample down to -210°C within an isothermal copper cell that can maintain a stable gas pressure in thermodynamic equilibrium with the sample at the same temperature. The chamber is designed to enable visible and near-IR monitoring throughout the physical evolution of ice samples thanks to sapphire windows (Grisolle 2013).

3 Methods

The concept of this work is to produce empirical experimental data to support the interpretation of data from orbital observations of the Martian SPC, namely the Compact Reconnaissance Imaging Spectrometer for Mars (CRISM) on board NASA's Mars Reconnaissance Orbiter

(MRO), which has a surface spatial resolution of around ~18m/pixel (Murchie et al., 2007), with a spectral resolution of ~6 nm.

3.1. Instrument parameters

The CRISM instrument has a resolution, of 9-19 nm full width at half maximum (FWHM) with 6.55 nm sampling over the 0.36-3.92 μm range (Murchie et al., 2007) In order to get a spectral resolution as close as possible to CRISM, we recorded spectra over the 0.7-3.6 μm spectral range using SHINE with a fixed slit of 1.5 mm, leading to 9-19 nm spectral resolution, and sampled every 10 nm (except for the first experiment sampled at 20 nm). To complete a full reflectance spectrum at this resolution took > 2.5 hours, so in order to effectively reduce the time between two spectra, especially during ice sublimation, in many instances multiple shorter spectra at wavelengths of interest were taken. The SHINE angular parameters used were fixed incidence angle = 0°, and observation angle = 20°, optimized for the CarboN-IR cell. This is comparable with a median phase angle of 0-30° for CRISM (Ceamanos et al., 2013).

3.2. Sample Preparation

Three samples were analysed for various ratios of PAHs mixed with CO_2 ice and two with finely ground Martian simulant JSC-Mars 1 (Allen et al., 1998). Much of the existing literature on PAHs found on icy moons and comets references the laboratory spectra recorded by Colangeli et al., (1992), which is pertinent to PAHs of astrophysical interest, rather than astrobiological, or specifically Martian. The six PAH species analysed by Colangeli et al., (1992) were benzene, chrysene, triphenylene, perylene, benzo [a] pyrene, pentacene and coronene. While chrysene and perylene have been found in Martian meteorites (Becker et al., 1997) and phenanthrene, pyrene, chrysene, perylene or benzopyrene and anthanthracene were found by McKay et al. (1996) the remaining four types of PAH have never been detected in Martian material. Therefore, we analysed our own mixture of PAHs based on those identified by McKay et al. (1996) in the ALH84001 and EETA79001 Martian meteorites but absent from Colangeli's analysis. The PAHs used were an existing mixture of anthracene ($C_{14}H_{10}$), phenanthrene-d10 ($C_{14}D_{10}$), and pyrene ($C_{16}H_{10}$) in raw form, obtained from Sigma-Aldrich (www.sigmaaldrich.com), in a 300 mg sample of equal parts of each PAH species. We will not discuss in this paper the bands due to or modified by the deuterated species as they do not contribute to PAH spectral features of interest.

In studies of Saturnian moons Iapetus and Phoebe (Cruikshank et al., 2008), the amount of PAHs detected on the surface was 10^{-4} to 10^{-3} g/cm^3 (0.01-0.1 %) so the first sample used 0.10 % PAH followed by 0.54 % and 0.67 % weight fractions for our three PAH samples mixed with CO_2 ice in order to allow the detection limit to be determined by plotting band depth as a function of concentration. The percentage amounts of PAH in CO_2 ice were difficult to fix precisely because some CO_2 ice sublimated during the process of mixing the materials, but they were precisely measured when the sample holder was filled with the prepared mixture, just before their introduction into the cell (see below). Increases in the amount of PAH for Samples 2 and 3 were chosen based on how well we could see the PAH features in Sample 1.

CO_2 ice was obtained from liquid decompression with a commercial device SnowPack©. This produces a granular snowpack of 312.5 cm^3 composed of small CO_2 ice grains. The average size of the grains, 150 μm, was estimated by measuring the true surface of the grains observed with a

binocular microscope (Philippe et al. 2016). Part of the CO_2 ice snow pack was then manually crushed, weighed, and a known mass of PAH powder was added and thoroughly mixed in a stainless-steel container pre-cooled with liquid nitrogen to limit CO_2 ice sublimation. The cell, also pre-cooled at -196°C, was filled up to its rim with the mixture (slightly compressed) and weighed before rapid installation inside the pre-cooled CarboN-IR environment chamber (-100 °C). The Martian South Pole's lowest temperatures can reach -153 °C and never exceeds -60 °C with the spring/summer temperatures for the SPC typically ranging between -80 and -100 °C (Smith, 2004); hence the choice to keep the environmental cell at the lower spring/summer temperature. The sapphire windows of the cryogenic chamber and of the external chamber were then successively closed and air was completely evacuated from both volumes by pumping using a detailed protocol developed to avoid frost condensation on the windows.

The grain sizes of our CO_2 ice samples are much smaller than what is generally observed on Mars South Polar Cap where CO_2 ice tends to have very coarse centimeter sized grains, generally in the form of compact slab (Douté et al. 2007). However, a major decrease in grain size, down to the millimeter, occurs after equinox (Langevin et al. 2007) and corresponds to the large increase of albedo oberved over the perennial cap during its sublimation phase. The grains in our samples are typically 5-10 times smaller than during the polar cap sublimation phase of interest. However, preparing such coarse grained CO_2 ice grains is a quite complex process and takes several weeks and was not possible given the experimental constraints (Philippe, 2016). But, as we will discuss later, using smaller grains may put stronger or weaker constraints on the detectability of PAHs, depending where their bands are situated relative to the CO_2 ice bands.

In addition, we measured one mixture of 1.5% PAH combined with a fine fraction (<25µm) of JSC-Mars 1 Mars simulant as well as this dust alone, as a reference.

The sample holder is 4.5 cm in diameter and 2 cm deep and has a total volume of 31.8 cm^3. Knowing the mass of the sample, measured just after filling the holder, and the density of bulk CO_2 ice (1.562 $g.cm^{-3}$) allowed to estimate the initial density and porosity of the sample, which is simply the fraction of the volume of the sample holder not occupied by CO_2 ice.

The percentage of H_2O ice mixed in the CO_2 snow was estimated (with uncertainty +/-20%) by comparison of its 1.5 µm band depth with that of the nearby CO_2 bands (at 1.435 and 1.58 µm) and relative to the spectra of a series of CO_2:H_2O ice mixtures previously measured and modelled (Philippe 2016). The mass fraction of H_2O ice in our samples is mostly of the order of the maximum values determined for the South Polar Cap, 0.08-0.12% (Douté et al. 2007) except in one case (~0.20%) where it exceeds these limits.

3.3. Experiment Protocol

After introduction of the sample holder containing the PAH-CO_2 ice mixture into the CarboN-IR cell and throughout the experiments, the cell and sample holder temperatures were kept at -100°C. Following initial measurements of the samples, sublimation experiments were conducted by pumping the CO_2 gas into the cell to monitor spectral and detection limit changes with sublimation. Bidirectional reflectance spectra (at single geometry) on both full Vis-NIR and

partial spectral ranges were recorded regularly during the sublimation experiment to reflect regions of interest for later comparison to observational results from orbital sensors.

4 Results

4.1. Preliminary Measurements

A first guess of the detectability limit for PAHs in CO_2 ice was established with reference to levels detected on other planetary bodies such as Iapetus, 10^{-4} to 10^{-3} g/cm^3 (Cruikshank et al., 2008). This was then tested at room temperature with a ~1% mix of PAH mixture with a transparent powder (alumine) in order to estimate the minimum amount of PAH required for detection within CO_2 ice but outside its absorption bands. From this preliminary experiment, an approximate detection limit of about 0.1% by weight was determined. This experiment also allowed us to define spectral ranges and resolution needed to detect the PAH mixture without interference from CO_2 ice spectra.

A spectrum of the 'pure' PAH mixture was also measured between 0.4 and 4.7 μm (at 20 nm sampling) as a reference (grey line in Figure 1). The positions and intensities of the bands are consistent with the reflectance spectra measured at higher spectral resolution up to 2.5 μm for our three PAHs by Izawa et al. (2014), except the 2.24 μm band which is much stronger in our PAH mixture spectrum.

Table 1 shows the details of the three CO_2 ice samples discussed in the subsequent sections.

Table 1: Sample Details

Sample No.	**Sample 1**	**Sample 2**	**Sample 3**
CO_2 Mass in g	31	23.5	30
PAH Mass in mg	32.7	158.1	161.6
Weight percentage of PAH to CO_2 in %	0.10	0.67	0.54
Weight percentage of H_2O to CO_2 in %	~0.12	~0.2	0.08
Weight fraction of PAH relative to H_2O	~0.8	~3.3	6.75
Density in g/cm^3	0.98	0.74	0.94
Porosity in %	38.5	52	40

4.2. PAH/CO_2 = 0.1% - Sample 1

For the first PAH+CO_2 ice sample, an amount of PAH comparable to our pre-estimated detection limit, 0.1%, was used. During this experiment the speed with which the interior chamber was pumped out from the ambient air resulted in water frost particles condensing on the surface of the sample being blown onto the inside of the window, and could not be removed (in the subsequent experiments this was done more slowly and with additional heating of the window to

avoid this problem) meaning that water contamination at the surface of CO_2 ice may be stronger in sample 1.

Two spectra were obtained from 0.4-3.6 μm with spectral sampling of 20 nm. As the vacuum was very stable, to aid sublimation, a lamp was used to heat the sample surface, at 27 cm distance from the window, resulting in 70W/m^2 equivalent to Mars at noon at 70° lat, achieving a sample sublimation of ~3 mm between two spectra. Upon examination of these spectra it was clear that the PAH feature at 3.29 μm is not observed on the side of the strong and broad 3.1 μm water ice band (the small shoulder at 3.32 μm is due to CO_2 ice), and so the following spectra were taken only between 0.6 and 2.0 μm at 20 nm sampling. Fig. 1 shows the results.

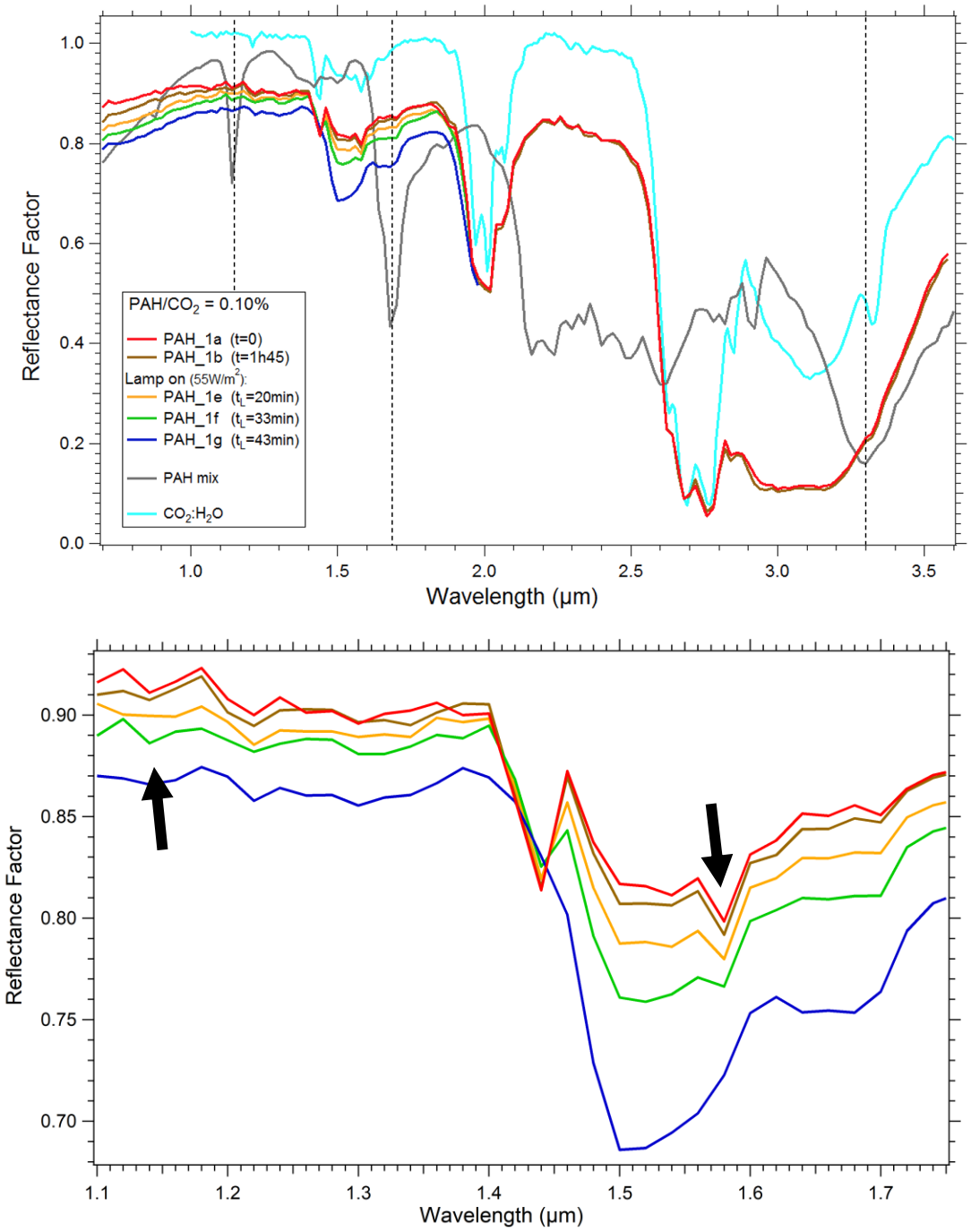

Figure 1: Top: Spectra from sample 1, 0.10% PAH in CO_2 ice (with small amount of H_2O ice ~0.12%) at -100°C during progressive sublimation of CO_2 (PAH_1a to 1g). Black, dotted vertical lines indicate the main infrared PAH absorption features. The sublimation was first free (1a, 1b) then triggered by illumination with a lamp (55W/m^2 at sample surface): 1e-1g. The spectrum of the PAH mix and of CO_2 ice (with small amount of H_2O ice ~0.075%) are also shown for reference. Note the increasing slope below 1.1 μm and the bands at the limit of detection at 1.14 and 1.685 μm. Bottom: Detail of PAH absorption features incicated by black arrows

It is clear over time, the overall reflectance of the spectra (PAH1a-1g) decreases as the CO_2 ice sublimates, and the slope increases between 0.7 and 1.1 µm. This is likely to be associated with the steep slope in the corresponding pure PAH mixture spectrum (black line) as sublimation increased the ratio of PAH/CO_2 ice and probably concentrated the PAH at the surface of the sample. We also notice that the water ice feature dominating around 1.52µm increases with sublimation, as the tiny frost particles present at very low level (~0.12%) in CO_2 ice are also segregated at the surface during sample sublimation (Philippe, 2016). A subtle absorption feature with a band depth of about 0.6% is visible in the PAH 1a-1g series of spectra corresponding with the pure PAH feature at 1.14 µm, with another weak feature visible at 1.68 µm (band depth ~ 1%). This latter band strongly increases in intensity during CO_2 sublimation and reaches an estimated depth of about 3% in the remaining PAH-H_2O ice lag deposit, but at this spectral sampling it is difficult to separate it from the 1.645µm band of H_2O ice. It would seem that the initial 0.10% PAH/CO_2 ice ratio is actually close to the detectability limit at this spectral resolution and sampling, and subsequent experiments used a higher initial ratio and a two times better spectral sampling to confirm the detection of the PAH bands.

4.3. PAH/CO_2 = 0.67% - Sample 2

For this second experiment, more care was taken to limit frost condensation at the surface of the CO_2 ice sample during transfer to the CarboN-IR cell and the ambient air was pumped more slowly to avoid window condensation or frost particles blown on it, but this was not successful as the water ice bands are about 2 times more intense than in Sample 1 with an estimated amount of H_2O ice of about 0.2%.

A higher spectral sampling, 10 nm, was used, meaning it took longer to obtain spectra, so a spectral range of 0.7-2.2 µm was chosen to obtain multiple spectra to observe the evolution of the features at 1.14 and 1.685 µm for the first 4 spectra (PAH2a-PAH2d) during the sublimating sequence. This limitation of the spectral range did not limit this study as CRISM spectra below 2.5 µm are the most useful for this work due to the interference of strong atmospheric water and ices features at 2.7-3.3 µm on Mars and because only the lower wavelength PAH features are detected against a background of CO_2 ice. There was a small leak in the cell, increasing sublimation rate, so the lamp was not used for sample 2 to reduce the sublimation rate of CO_2. The spectral range was then increased to 0.7-2.75 µm and left to run overnight, resulting in total of 6 spectra, shown in Fig. 2.

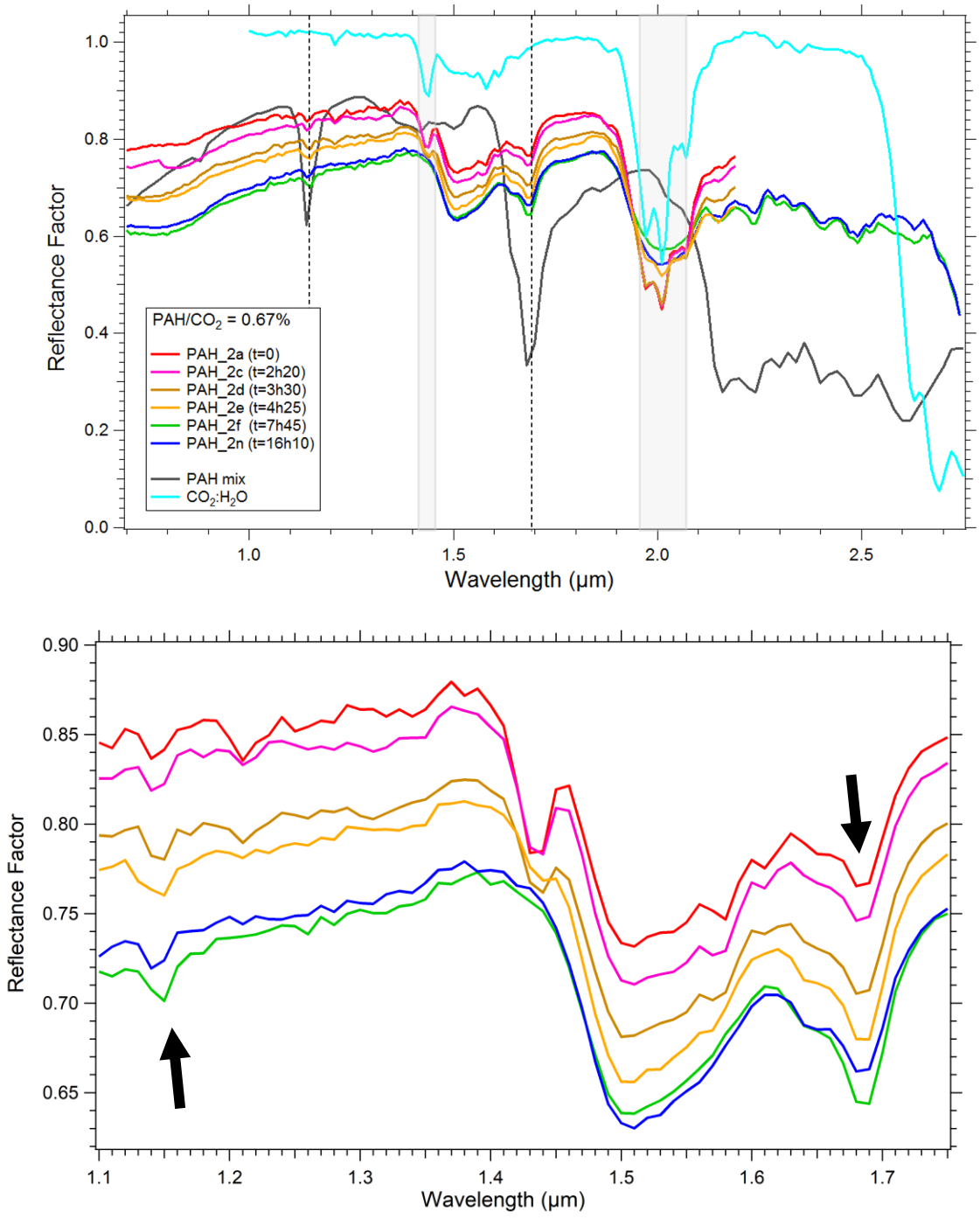

Figure 2: Top: Spectra from sample 2, 0.67% PAH in CO_2 ice (with small amount of H_2O ice ~0.2%) at -100°C during progressive sublimation of CO_2 (PAH_2a to 2n). Black, dotted vertical lines indicate the main infrared PAH absorption features, transparent grey boxes indicate transforming CO_2 ice absorption features. The sublimation was free until the complete disappearance of CO_2 ice. The spectrum of the PAH mix and of CO_2 ice (with small amount of H_2O ice ~0.075%) are also shown for reference. Note the increasing slope below 1.1 µm and the bands clearly appearing at 1.14 and 1.685 µm, but also in the 2.1-2.6 µm range. Bottom: Detail of PAH absorption features incicated by black arrows

With the increased amount of PAH in the ice, the absorption features at 1.14 and 1.685 μm (band depths of 2% and 7% in the mixture, respectively) are now clearly visible throughout all PAH/CO_2 ice spectra, as well as the slope at 0.7-1.1 μm. In the extended spectra PAH2e-PAH2p, there are also corresponding features visible at 2.15, 2.24, 2.29, 2.33, 2.41, 2.49 and 2.62 μm in pure PAH and PAH/CO_2 ice spectra. It is also clear that with the increased initial amount of H_2O ice in this sample (~0.2%, instead of ~0.12% in Sample 1) the CO_2 ice absorption feature at 1.435 μm and its triplet features around 2 μm become more rapidly dominated by the strong and broad 1.5 and 2 μm absorption bands of water ice, as CO_2 ice sublimates. When all the CO_2 ice has sublimated, leaving only a thin deposit (~170 μm) of water ice-dust mixture, the intensity of both the 1.14 and 1.685 μm bands have increased by about 70%, and then started to decrease slowly while the H_2O ice band was stable.

4.4. PAH/CO_2 = 0.54% - Sample 3

For this experiment a spectral range of 0.4 -2.75 μm was chosen with resolution of 10nm. Details of sample 3 are shown in table 1. This time with an improved preparation protocol we succeeded in efficiently suppressing any additional condensation of frost at the surface of the CO_2 ice, and the water ice content (0.08%) is now similar to what was previously achieved for pure CO_2 ice, as witnessed by the almost identical ratio between the 1.52 μm band of H_2O and 1.435 μm band of CO_2 ice in the initial spectrum 3a (Figure 3).

Sixteen spectra were taken throughout the day and overnight during the sublimation sequence. As with experiment 1, the vacuum was very stable, and slow sublimation occurred, resulting in fairly homogenous spectra. Results are shown in Fig. 3.

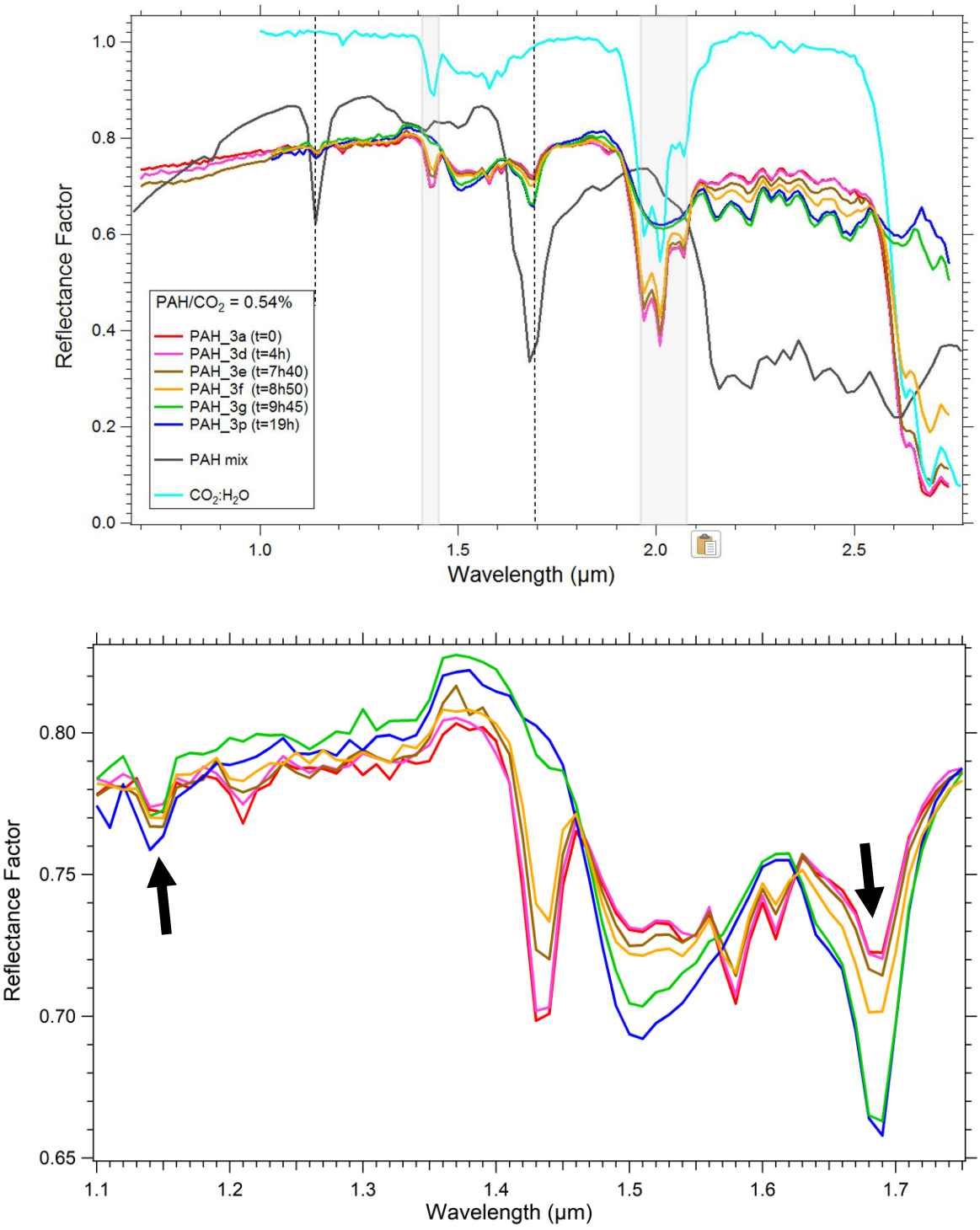

Figure 3: Top: Spectra from sample 3, 0.54% PAH in CO_2 ice (with small amount of H_2O ice ~0.08%) at -100°C during progressive sublimation of CO_2 (PAH_3a to 3p). Black, dotted vertical lines indicate the main infrared PAH absorption features, transparent grey boxes indicate CO_2 ice absorption features mentioned in the text. The sublimation was free until complete disappearance of CO_2 ice. The spectrum of the PAH mix and of CO_2 ice (with small amount of H_2O ice ~0.075%) are also shown for reference. Note the increasing slope below 1.1 µm and the bands clearly appearing at 1.14 and 1.685 µm, but also in the 2.1-2.6 µm range. Bottom: Detail of PAH absorption features incicated by black arrows.

With 0.54% PAH, the features at 1.14, 1.685, 2.15, 2.24, 2.41, 2.49 and 2.62 μm are visible as with sample 2. With these higher signal-to-noise spectra, it is also possible to better observe the replicated PAH features at 2.29 and 2.33μm, with the PAH/CO_2 ice mixture between 2.1 and 2.5μm closely mirroring the shape of the spectrum for pure PAH mixture. The change in the slope at 0.7-1.1 μm is also clear but unfortunately was not monitored until the end of the experiment. Again as with Sample 2, the CO_2 ice absorption feature at 1.435 μm becomes muted with sublimation, but the triplet feature at ~2 μm is less affected in the first stages of sublimation with an initial 'contamination' of only 0.08% water ice, as was the case with the small amount of H_2O ice in Sample 1. During CO_2 sublimation, the intensity of the 1.14 μm band increased by about 50%, and that of the 1.685 μm by a factor of 2.3 when only a H_2O ice-dust sublimation residue remained at the bottom of the sample holder (only about 120 μm thick). Other bands, such as those of 1.155 μm and 2.49 μm, increased by an even greater proportion.

4.5. PAH/dust = 1.52% and dust - Samples 4 and 5

A final experiment, with two spectra ranging from 0.4-3.9 μm at a resolution of 10nm, was taken of the PAH mixture in Mars simulant JSC Mars-1, weathered volcanic ash from Hawaii (Allen et al., 1998), as well as a pure dust spectrum for reference (Figure 4). The JSC Mars-1 regolith simulant was previously ground and sieved below 25 μm to simulate Martian atmospheric dust. Sample details are shown in Table 2.

Table 2: Details of Samples 4 and 5

Sample Description	**Sample 4 : PAH/ JSC Mars-1 Dust Mix**	**Sample 5: JSC Mars-1 Dust**
Dust Mass in g	7.7	15.4
PAH Mass in mg	117	-
Weight percentage of PAH to dust in %	1.52	-
Density in g/cm^3	1.895	1.91
Porosity in %	48.1	49.3

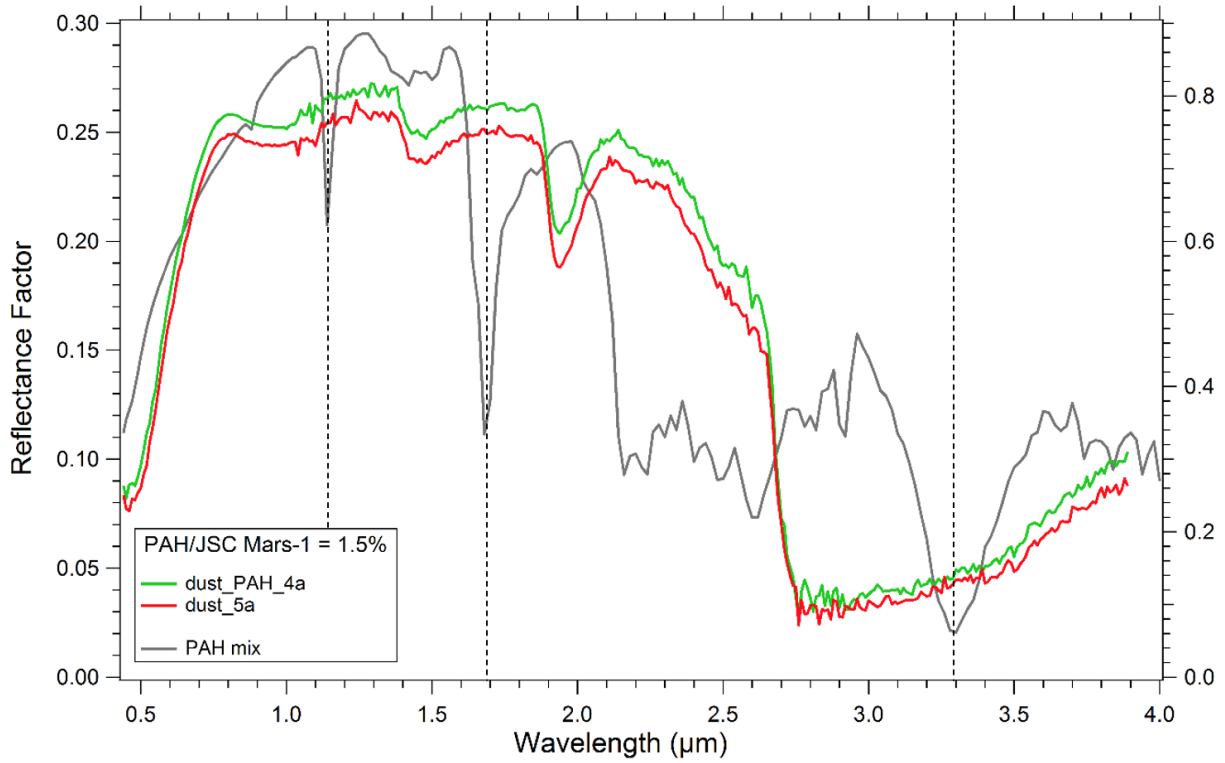

Figure 4: Spectra from samples 4 and 5, 1.52% PAH in JSC Mars-1 (dust_PAH_4a), and JSC Mars-1 (dust_5a) at room temperature. Black, dotted vertical lines indicate the main infrared PAH absorption features. The spectrum of the PAH mix is also shown for reference (right scale). Note that no sign of increase of slope below 1.1 μm and no bands are detected at 1.14, 1.685 μm, nor at 3.29 μm,

Despite PAH particles being clearly visible in the physical sample, and the ratio of PAH to substrate being 2.5 to 3 times higher than in ice samples 2 and 3, (1.52% compared to 0.67% and 0.54%), no spectral features of PAHs were detectable in the dust spectrum.

Other than the pure dust sample being slightly lower in overall reflectance, there is no observable difference in spectra between pure dust and PAH/dust mix. This is most likely because of the relative opacity of dust compared with CO_2 ice, its continuum reflectance being three times lower. If PAHs are not discernible in Martian dust at concentrations an order of magnitude higher than that detected on Iapetus, it is likely to be an extremely limiting factor in detecting PAHs on the SPRC if any potential PAHs are mixed with dust and not in pure form. No known segregation process can concentrate PAH in dust as is the case with PAH/CO_2 ice mixtures. In order to ascertain whether PAHs in small amounts of dust are detectable when mixed in CO_2 ice, further experiments will need to be carried out to better emulate the scarp wall dust deposits in SCT. However, with our current set of experiments, it is already possible to make some

extrapolations on the detectability of PAH in materials with different compositions encountered on the South polar cap and in the water ice-dust lag deposits at its margins.

5 Discussion

The results of these novel experiments are extremely useful to allow a future new analysis of orbital observations from the CRISM instrument on Mars Reconnaissance Orbiter, and establish a detection limit for PAHs in CO_2 ice and in H_2O ice-dust lag deposits, not only at the poles, but in shadowed regions elsewhere, in sub-surface ice that may be sampled during future exploration missions as well as on icy bodies. In addition, we ascertained the limitations of observing PAHs directly in 'dry' Martian regolith, a first step towards establishing the detectabililty of PAH in the regolith of other planets. This study also provides more relevant bi-directional reflectance data in the near-infrared range on diagnostic PAH signatures of astrobiological importance to Mars, that are pertinent to planetary ices, as most previous literature, except Izawa et al. (2014), used mid-infrared transmission data from the 1990s which is more relevant to interstellar dust cloud PAH detection.

PAHs are extrememly important to theories of abiogenesis, and while their presence is ubiquitous in space, their detection on planetary bodies remains a major objective in planetary science. The attempt to detect them on Mars is worthwhile given the recent discoveries of other organic compounds and subterranean lakes (Freissinet et al., 2015; Ojha et al., 2015; Orosei et al., 2018).

In the spectrum of our mixture of three PAHs the strong 1.685 μm band is the first overtone ($2\nu_{CH}$) of the fundamental aromatic symmetric C-H stretch modes (ν_{CH}) occurring at ~3.29 μm. From the position of these two bands, we deduce that the 1.14 μm band is the second overtone ($3\nu_{CH}$) of these modes, and the weak band at 0.88 μm is the third overtone ($4\nu_{CH}$) (Izawa et al. 2014). The other bands between 2.1 and 2.9 μm are mostly combination bands between these stretching modes and various types of aromatic C=C deformation modes and C-H stretching and bending modes. Due to the use of phenanthrene-d10 in our sample there are also additional bands at 2.24 and 1.50 μm due to the first and second overtone of the fundamental C-D stretch modes. Weaker bands between 1.30 and 1.55μm are higher order combinations (Izawa et al. 2014). In our discussion we will only consider the 1.14 and 2.685 μm C-H stretch overtone bands.

5.1 Detectiability of PAH in CO_2 ice

We have shown that the most interesting and sensitive signature of PAH for detection on the Mars residual CO_2 ice cap is this $2\nu_{CH}$ band at 1.685 μm, well outside the CO_2 ice bands and the strongest H_2O ice bands (Figure 6). The only band that can slightly interfere with this PAH band is the 1.645 μm band of water ice, which is seen in our spectra as a weak shoulder on the low wavelength side of the PAH band (see e.g. Figure 2). However, it is shifted to lower wavelengths by 0.04 μm, well above the resolution of all current and future near-infrared spectrometers. We found that even with more than 0.1% water in CO_2 ice, which is rarely the case in the very dry southern hemisphere (Douté et al. 2007 found 0.02-0.12% H_2O in CO_2 ice), this ice band did not preclude the detection of PAH homogeneously mixed at levels below 0.1% in CO_2 ice.

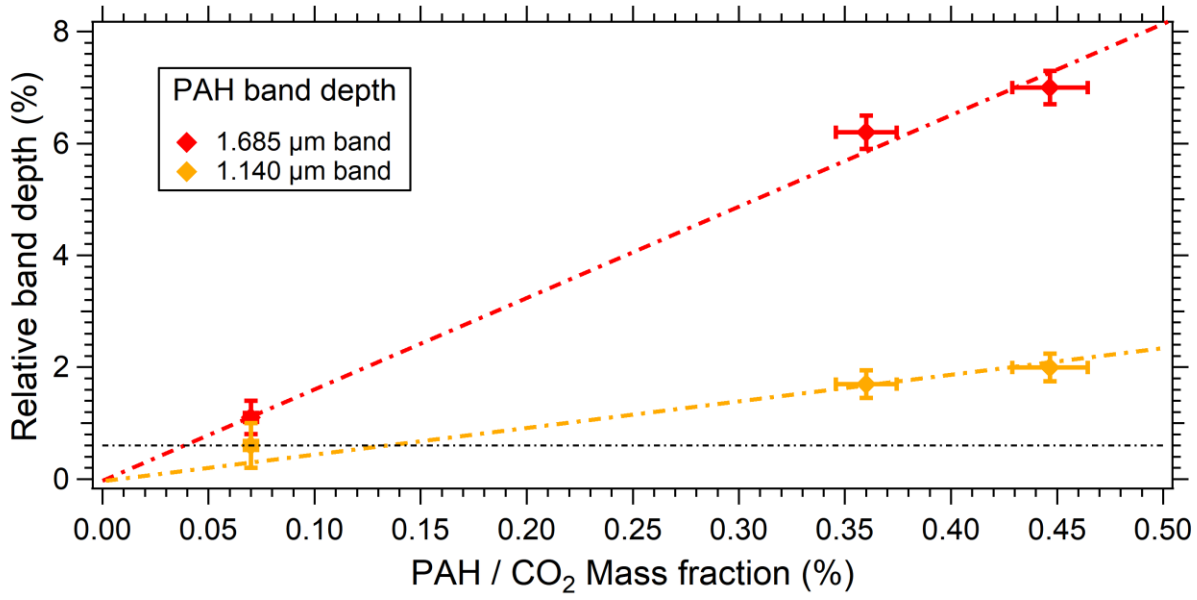

Figure 5: Relative band depth of the 1.14 and 1.685 µm bands of PAH versus the mass fraction of PAH (contributing to these aromatic C-H stretching bands) of the initial homogeneous mixture in CO_2 ice at -100°C. The horizontal line represents a band depth detection level of 0.6% (at 3σ with S/N=450-500).

In order to better assess the detectability level of this band and the 1.14 µm one for PAH homogeneously mixed with CO_2 ice (before any sublimation), we have plotted in Figure 5 the initial relative band depth of both bands versus the mass fraction of PAH containing C-H bonds (removing phenanthrene-d10 which did not contribute to these bands). Assuming the pre-flight SNR value of 450-500 around 1.14 and 1.68µm given for CRISM (Murchie et al., 2007, Fig. 33b), the detection level of these bands in an observed spectrum with reflectance close to 1 (as for CO_2 ice) is for a band depth of 0.6% relative to the nearby continuum (i.e. for a 3σ detection level, horizontal dotted line in figure 5). The detectability of the 1.685 µm band of PAH well mixed in fine grained CO_2 ice (D ~150 µm) is thus at about 0.04% PAH weight fraction, and that of the 1.14 µm at about 0.13%. The detection level for the 1.685 µm band should be only slightly affected at the lower temperature of the SPC (~-150°C), whereas the 1.645 µm H_2O band gets stronger and shifts slightly towards the PAH band (see Fig 2 of Grundy and Schmitt, 1997; 1998). The 1.14 µm band is weaker but, on the other hand, absorbs at a wavelength without CO_2 absorption and between two much weaker water ice bands.

The slope between 0.7 and 1.1 µm, and the absorption features in the 2.1-2.5 µm range may also provide additional clues to confirm detection. The visible slope of PAH occurs in a range of full transparency of both ices, but it cannot be used as a detection criteria as it may be confused with the slope induced by a small amount of contaminating reddish dust. The bands between 2.1 and 2.5 µm are also mostly outside any strong CO_2 absorption and are clearly observed in most of our spectra, down to a PAH abundance at 0.1% level, despite a larger abundance of H_2O ice in our samples compared to the Mars South Polar Cap. However, the two generally weak CO_2 ice

bands at 2.295 and 2.35 µm may become much stronger in some situations (larger grain size, see e.g. Douté et al. 2007; Langevin et al. 2007) and strongly interfere with this set of PAH bands.

On the other hand, the 'classical' strong 3.29 µm fundamental band of PAH interferes with the relatively strong 3.32 µm band of CO_2 ice but is also buried in the wing of the strong water ice band at 3.1 µm which can saturate even with a very small amount (<< 0.1%) of H_2O trapped in CO_2 ice (see e.g. Figure 1). Similarly, when mixed with martian soil this band falls in the wing of the very strong band of both structural and adsorbed H_2O. This 3.29 µm band thus cannot be used to detect PAH in reflectance spectra of icy surfaces.

An important point to consider here is the difference in CO_2 ice grain sizes between our samples (~150 µm) and the perennial cap: from several centimetres (clear compact slab) decreasing down to a few millimeters during sublimation in spring (Langevin et al. 2006, Douté et al. 2007). Larger grains increase the intensity of the CO_2 absorption bands and can efficiently hide any other signatures there on in their wings, but on the other hand, such large grains allow light to penetrate and probe much deeper in the wavelength ranges outside the relatively narrow CO_2 bands. In particular, the 1.685 µm PAH band is situated at a wavelength where the absorption coefficient of CO_2 is extremely low (< $3\ 10^{-4}$ cm^{-1}; Quirico and Schmitt 2004, Hansen 2005). So it is anticipated from radiative transfer considerations that the detection level of this PAH band should be largely improved in such coarse grained or slab ice, possibly down to the 0.01% level. The main limitation will come from the abundance of water ice which has an absorption coefficient around 10 cm^{-1} at 1.685 µm (in the wing of the 1.645 µm H_2O band) for pure ice (Grundy and Schmitt, 1997; 1998), i.e. about 4 orders of magnitude above that of CO_2 ice. A water ice abundance above a few percent should preclude the detection of trace amounts of PAH at this wavelength. On the other hand the 1.14 µm band is situated at a wavelength of minimum absorption of H_2O ice (~ $5\ 10^{-2}$ cm^{-1}) and may be a better probe where H_2O ice is moderately abundant.

Also, as CO_2 ice sublimates, the PAH contained in the sublimated layers segregates at its surface together with H_2O ice and its band depth progressively increases by a factor which depends on the initial amount of H_2O ice. This increase is only by a factor of 1.55 when the H_2O/CO_2 ratio is large, as for sample 2 (0.20%), but can reach a factor of 2.3 when this ratio is small, as for sample 3 (0.08%). So the 'visibility' of PAH is increased by the CO_2 sublimation only until a mix of PAH and H_2O ice remains. On Mars the accumulation factor of PAH at the surface (at the same initial concentration) will be larger as the thickness of sublimated CO_2 is more than an order of magnitude larger than for our sample (2 cm).

5.2 Detectability in the PAH-H_2O ice lag deposit

Another important result is that for all our samples, the PAH bands are still observed in the H_2O-PAH mixture left over after complete sublimation of the CO_2 ice, and with an increased intensity despite the relatively high initial content in H_2O ice (0.08-0.20%) relative to the Mars South Polar Cap. Our three resulting sublimation lag deposits have H_2O/PAH ratios ranging from 15 to 120% (see Table 1) and display very clear and strong PAH bands at all wavelengths for Samples 2 and 3 (Figures 2 and 3). Even for Sample 1, where H_2O ice dominates the composition of the

mixture, the 1.685 µm is easily detectable, although blended with the 1.645 µm H_2O band (but the sampling was only 20 nm for this sample) which now has a similar intensity (see the blue curve in figure 1). Its relative band depth is about 3%. So PAH may still be detectable in the lag deposit, as a shoulder ~1% deep on the side of the 1.645 µm band, if the initial weight abundance of PAH relative to H_2O ice is more than about 25% (~3 times less than for Sample 1). Given the average concentration of 0.02-0.04% for H_2O ice in CO_2 ice determined for the dry ice-rich terrains (Douté et al. 2007) at Ls~140°, we can still expect to be able to detect PAH mixed with pure H_2O ice in the sublimation lag deposit when PAH is present in the initial CO_2 ice down to a concentration as low as 0.005-0.01%.

In our experiment, we did not find a good correlation between the PAH band depths and the PAH/H_2O ice weight ratio, but rather some correlation with the PAH mass column in the sample (Figure 6). This is probably due to the fact that this lag deposit is very thin (65-170 µm, assuming a porosity of 50%) and thus probably still optically thin in these bands. In our experiments a mass column of 0.3 mg/cm^2 may be derived as the 0.6% band depth detection level (for CRISM SNR, see 5.1) for PAH in PAH-H_2O mixtures. However, for optically thick water ice deposits, as on Mars, this may be underestimated. These estimates call for future experiments to measure the actual level of detectability of PAH mixed with water ice.

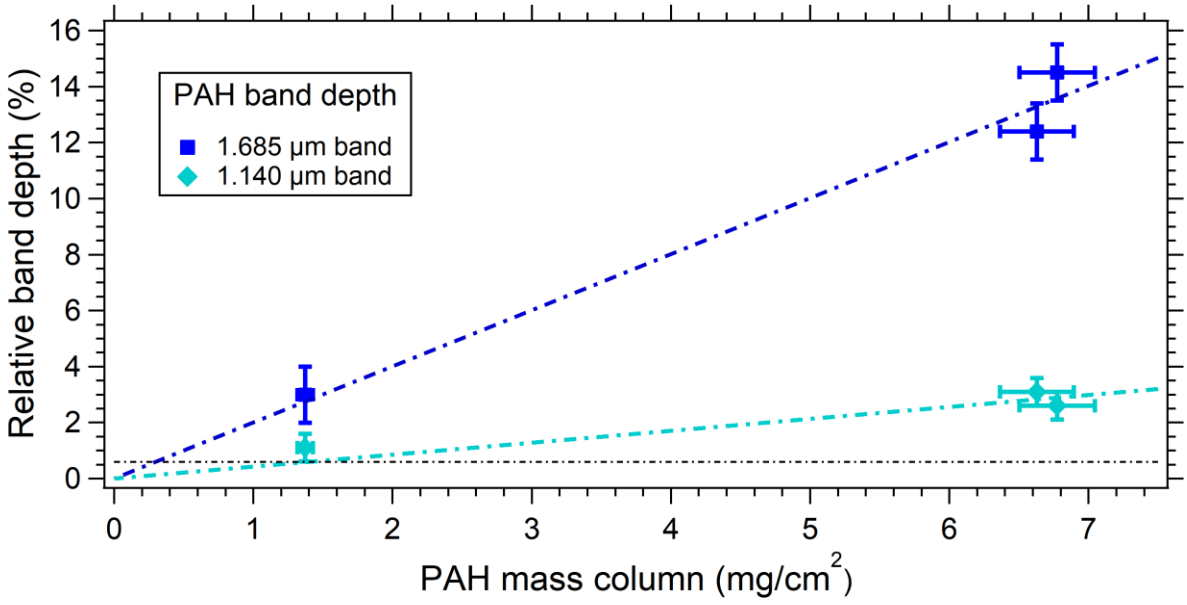

Figure 6: Relative band depth of the 1.14 and 1.685 µm bands of PAH versus the mass column of PAH (contributing to these aromatic C-H stretching bands) in the PAH-H_2O ice sublimation lag deposit. The horizontal line represents a band depth detection level of 0.6% (at 3σ with S/N=450-500).

5.3 Effect of dust on the detectability of PAH

As we already saw with our single experiment of PAH-dust mixture, the limitation on the detectability of PAH is also strongly constrained by the amount of dust present in the ice. Indeed the martian dust aerosol particles that are mixed with CO_2 ice have strong absorption coefficients over all the near infrared range (in the range 30-120 cm^{-1} @ 1.14 µm, 50-180 cm^{-1} @ 1.685 µm

and increasingly larger above; Douté et al., 2007), so one to three orders of magnitude larger than for H_2O ice and four to six orders larger than for CO_2 ice at the wavelengths of these PAH absorptions. Furthermore, aeolian dust has a much smaller grain size (<10 µm) and therefore, in addition to strongly absorbing light, it will scatter it efficiently and reduce the probed depth. The non-detection of 1.5% PAH in a fine fraction (< 25 µm) of JSCMars-1 analogue is most likely an underestimate of the detection limit of PAHs in dust.

On Mars a small amount of dust is mixed with CO_2 ice on the South Polar Cap. Its concentration has been estimated in the 0.02-0.14% range with a dust/H_2O ratio ranging between 0.5 and 4 in the CO_2 ice-rich terrains (Douté et al. 2007). These authors also derived very similar dust/H_2O ratios for the water ice-rich terrains on the margins of the cap, as expected after sublimation of the CO_2 ice.

Considering the similarity in absorption coefficient between dust and the strong absorption peak at 2µm of H_2O ice (~100 cm^{-1}), a high abundance of dust (~0.14%) mixed with CO_2 ice will certainly cancel the positive effect of larger CO_2 grain size and limit the detectability of PAH to a higher level than our measured value of 0.06%, possibly closer to 1%. The reflectance of such types of dusty CO_2 ice is only slightly larger (by ~30%) than for the surrounding 'dry' terrains (Douté et al. 2007). So penetration of light is already quite limited. But if dust is present in lower amounts (~0.02-0.04%, reflectance almost twice that of dust) the penetration depth of light in slab CO_2 ice should allow a lower detection limit for PAHs.

In the PAH-H_2O-dust sublimation lag deposit a similar degradation of the detection level should occur depending on the dust/ H_2O ratio. If it is at its lower limit (~0.3) the effect should be mostly to reduce the reflectance in the continuum absorption and thus reduce the detectability of the 1.14 µm band and significantly affect the visible slope, but this will only partly reduce the relative band depth of the 1.685 µm band. For higher concentrations of dust relative to both CO_2 and H_2O ice, its effect is likely to strongly reduce the detection level of PAH, possibly up to ~1% for the largest observed dust/H_2O ratio ~4 (Douté et al. 2007).

All these results and rough estimates based on relative values of absorption coefficients call for experiments to directly measure the detectability of PAHs in mixtures of PAH/dust/H_2O ice dispersed in small amounts in slab CO_2 ice and as sublimation lags in order to better assess both the boosting effect of large CO_2 grain size and the deleterious effects of dust. Radiative transfer models may also help us to understand the detection limits both in experiments and in observations.

5.4 Extrapolation to other PAHs

Another important question now arises about the wider applicability of our experiments with a selection of only three of the simplest PAHs in comparison to other more complex molecules in this family.

It is established that in PAHs the symmetric C-H stretching modes are of two types (for 'bay' and 'non-bay' hydrogen atoms; Baushlisher et al; 2009) but are non-specific of the particular PAH molecule (which show only slight wavelength shifts). They occur in all the members of this family but in different proportions depending on the compactness of the PAH, the 'non-bay H

being generally dominant (100% in anthracene and pyrene, 80% in phenanthrene). For the fundamental stretching modes, the two bands occur respectively in the 3.205-3.23 µm (bay H) and 3.23-3.28 µm (non-bay H) ranges for the gas phase, and slightly shifted to higher wavelength in the condensed phase. Accordingly, from a study of the visible-near-infrared reflectance spectra of 47 simple and substituted PAHs in the solid state, Izawa et al. (2014) showed that the overtone bands have mostly one major band (as we observed too) and their positions are relatively well constrained in a narrow range: 1.138-1.150 µm for $3\nu_{CH}$ and 1.673-1.690 µm for $2\nu_{CH}$ mode, with a small shoulder in the range 1.645-1.650 µm.

Depending on the exact PAH or mixture, its detectability from the $2\nu_{CH}$ 1.685 µm band may therefore be only slightly decreased if the band shifts to the lower limit of its wavelength range (more interference with the 1.645 µm H_2O ice band) but will increase if its peak shifts away from this band. For the $3\nu_{CH}$ band, no effect on detectability is expected as there is no interfering band nearby. All these shifts have no effects for the detectability in dust as the aeolian dust spectrum display no features in these ranges having a quite flat spectrum.

Another factor that may affect detectability (by weight %) is the H/C ratio of the molecule or the PAH mixture. In our mixture this ratio is relatively low (0.45) due to the use of one deuterated molecule. It is similar to the values for larger compact PAH molecules, e.g. 0.5 for coronene ($C_{24}H_{12}$), and lower than for the small PAHs found in Martian meteorites (Becker et al., 1997): 0.6 for chrysene ($C_{18}H_{12}$), 0.625 for pyrene ($C_{16}H_{10}$), 0.67 for perylene ($C_{20}H_{12}$) and 0.71 for both anthracene and phenathrene ($C_{14}H_{10}$). But these differences are quite small compared to the previously discussed radiative transfer effects controlling the detectability of PAHs.

Only if some aromatic C=C bonds in the PAH material are eliminated, either by substitution (by oxygen atoms, OH, CH_3, …) or by hydrogenation, will the number of aromatic C-H stretching modes decrease, and consequently the strength of both the 1.14 and 1.685 µm bands. In the last case (H_n-PAHs) new, intrinsically stronger, aliphatic C-H stretching modes will appear at higher wavelength, shifted by +0.10-0.26 µm for the fundamental modes (Sandford et al. 2013) and thus by about +0.05-0.13 µm for the first overtone, and + 0.03-0.09 µm for the the second, as observed by Izawa et al. (2014). Their first overtone will be easier to observe as it will shift towards the minimum absorption between the 1.645 µm and the broad 2-µm water ice bands, but it will be the reverse for the second overtone as it will shift in the wing towards the peak absorption of the 1.26 µm H_2O band. However, this particular family of PAH molecules has not been studied in our experiments.

6 Conclusions

To summarise: a detectability limit of ~0.04% has been established for observing PAH features in sublimating CO_2 ice but this detection limit may drop by a large factor (to ~0.01%) in coarse grained ice if the amount of dust is at its lowest values (~0.02%) measured on the South Polar Cap. On the other hand, even at its maximum detected concentration in CO_2 ice (~0.12%), water ice should have only a limited effect on the detectability of PAHs.

Similarly in the PAH-H_2O-dust lag deposits observed on the SPC margins and rim scarps the amount of dust is the main factor that may strongly limit the detectability of PAH (up to only 1%

in the original CO_2 ice) while in dust-poor PAH-H_2O lag deposits PAHs can be detected when the PAH/H_2O ice ratio is larger than 25%, i.e. for initial PAH concentration in CO_2 ice in the range 0.01-0.05 %.

These detectability limits are roughly applicable to most types of C_nH_n PAHs as the two diagnostic bands only slightly change in position and specific band strength among this PAH family. If other PAH families (substituted, hydrogenated…) are present on Mars or other icy bodies, then specific studies of their mixtures with CO_2 or H_2O ice and dust should be performed to assess their detection limits in specific environments.

The detectability levels achievable in the near-infrared in favorable conditions on Mars are thus of the same order than the amount detected on other planetary bodies, i.e., 10^{-4} to 10^{-3} g/cm3 (Cruikshank et al., 2008). One particular advantage of the near infrared bands may be that they allow us to probe deeper into the surface (up to few millimeters or centimeters for clear CO_2 ice slab) than just the very first microns seen by the 3.29 µm PAH band.

When future space observations of the SPC are recorded at higher spectral resolution & sampling than our measurements (19 nm/10 nm) the better separation between the relatively narrow 1.685 µm PAH band and the 1.645 µm H_2O ice band will further improve the PAH detectability.

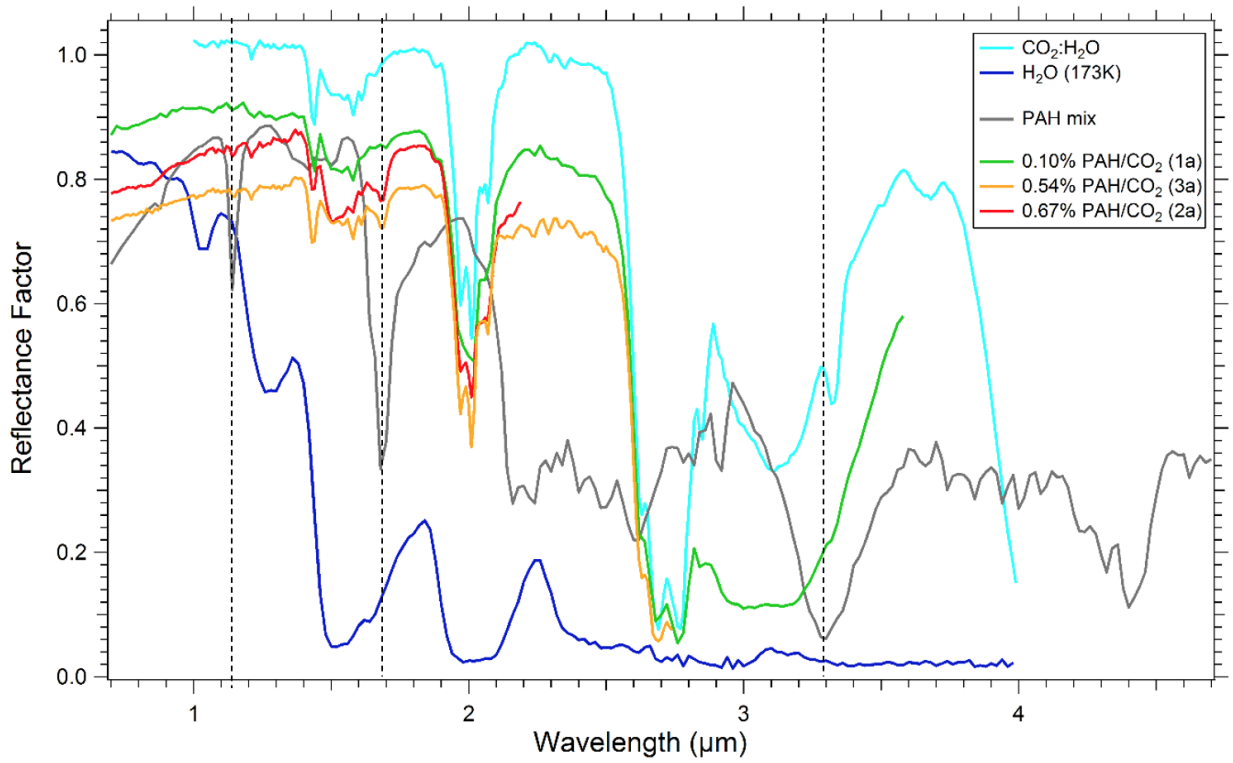

Figure 7: Spectra from three initial samples (1a, 2a, 3a) with varying amount of PAH in CO_2 ice (with small amount of H_2O ice ~0.08-0.2%) compared to the spectrum of the PAH mix and with those of CO_2 ice (with ~0.075% H_2O ice) and pure H_2O ice at 173K (Philippe 2016). Black, dotted vertical lines indicate the main infrared PAH absorption features.

Analysis of Mars spectra and computer modelling will be carried out in future to apply the empirical laboratory results to CRISM observations, and further laboratory work is planned to obtain PAH spectra pertinent to non-polar regions of Mars. Detectability of PAHs in pure and 'contaminated' water ice has far reaching consequences for other planetary bodies such as comets, Europa, Enceladus and Titan, the study of which would greatly benefit from being able to discriminate the effects of PAH and ice on spectra, and comparison with PAH libraries.

Acknowledgments, Samples, and Data

The measurements described in this work are the outcome of the Trans-National Access research project "Laboratory Analysis of Martian South Polar Residual Cap Analogues for Comparison with CRISM Observations" selected and funded in the framework of the Europlanet 2020 RI program (http://www.europlanet-2020-ri.eu). Europlanet 2020 RI received funding from the European Union's Horizon 2020 research and innovation programme under grant agreement No 654208.
The lead author is supported by MSSL STFC Consolidated grant no. ST/K000977/1 STFC under PhD studentship no. 526933.
The complete set of data presented in this paper (Campbell et al., 2017) is available online upon publication of this paper in the CSS database of the SSHADE database infrastructure (https://www.sshade.eu/db/css):
https://doi.org/10.26302/SSHADE/EXPERIMENT_BS_20181101_001

References

Allamandola, L.J. (2011). *PAHs and Astrobiology*. PAHS and the Universe, EAS publications series, 46. pp.305-317

Allen, C.C.; Morris, R.V.; Jager, K.M.; Golden, D.C.; Lindstron, D.J.; Lindstrom, M.M.; Lockwood. J.P. (1998). *Martian Regolith Simulant JSC Mars-1*. Lunar and Planetary Sciences XXIX.

Bauschlicher Jr., C. W., E. Peeters, and L. J. Allamandola (2009). *The infrared spectra of very large irregular polycyclic aromatic hydrocarbons (PAHs): observational probes of astronomical pah geometry, size, and charge.* The Astrophysical Journal, 697:311–327,Becker L., Glavin D.P., Bada J.F. (1997). *Polycyclic aromatic hydrocarbons (PAHs) in Antarctic Martian meteorites, carbonaceous chondrites, and polar ice*. Geochimica et Cosmochimica Acta, 61, pp. 475-481.

Benner, S.A., Devine, K.G., Matveeva, L.N. and Powell, D.H., (2000). *The missing organic molecules on Mars.* Proceedings of the National Academy of Sciences, *97*(6), pp.2425-2430.

Bonnefoy N., Brissaud O., Schmitt B., Douté S., Fily M., Grundy W., Rabou P. (2000). *Experimental system for the study of planetary surface materials - BRDF*. Remote Sensing Reviews, 19, 59-74.

Botta O. and Bada J. (2002). *Extraterrestrial organic compounds in meteorites*. Surveys in Geophysics 23, pp.411–467.

Brissaud O., Schmitt B., Bonnefoy N., Douté S., Rabou P., Grundy W., Fily M. (2004). *Spectrogonio radiometer for the study of the bidirectional reflectance and polarization functions of planetary surfaces.* Applied Optics 43, No. 9.

Byrne, S. (2009). *The Polar Deposits of Mars*. Annual Review of Earth and Planetary Science, 37. pp.535-560

688 Campbell, Jacqueline; Schmitt, Bernard; Beck, Pierre; Brissaud, Olivier (2017): *Vis-NIR reflectance spectra of a mix*
689 *of three PAHs, PAHs mixed with CO_2 snow and PAHs mixed with JSC Mars-1 simulant*. SSHADE/CSS (OSUG Data
690 Center). Dataset/Spectral Data. doi:10.26302/SSHADE/EXPERIMENT_BS_20181101_001
691 Campbell, J.D., Sidiropoulos, P. and Muller, J.P., 2018. *A search for polycyclic aromatic hydrocarbons over the*
692 *Martian South Polar Residual Cap.* Icarus, 308, pp.61-70.
693 Ceamanos, X., Douté, S., Fernando, J., Schmidt, F., Pinet, P. and Lyapustin, A., 2013. *Surface reflectance of Mars*
694 *observed by CRISM/MRO: 1. Multi-angle Approach for Retrieval of Surface Reflectance from CRISM observations*
695 *(MARS-ReCO*). Journal of Geophysical Research: Planets, 118(3), pp.514-533.
696 Cockell, C.S. Catling, D.C. Davis, W.L. Snook, K. Kepner, R.L. Lee, P. McKay, C.P. (2000). *The ultraviolet*
697 *environment of Mars: Biological Implications past, present and future*. Icarus. 146. 343-359
698 Colangeli, L. Mennella, V. Baratta, G.A. Bussoletti, E. Strazzulla, G. (1992). *Raman and infrared spectra of polycyclic*
699 *aromatic hydrocarbon molecules of possible astrophysical interest*. The Astrophysical Journal. 396. 369–377.
700 Cruikshank, D.P. Wegryn, E. Dalle Ore, CM. Brown, R.H. Bibring, J-P. Buratti, B.J. Clark, R.N. McCord, T.B.
701 Nicholson, P.D. Pendleton, Y.J. Owen, T.C. Filacchione, G. Coradini, A. Cerroni, P. Capaccioni, F. Jaumann, R.
702 Nelson, R.M. Baines, K.H. Sotin, C. Bellucci, G. Combes, M. Langevin, Y. Sicardy, B. Matson, D.L. Formisano, V.
703 Drossart, P. Mennella, V. (2008). *Hydrocarbons on Saturn's satellites Iapetus and Phoebe*. Icarus. 193. 334-343
704 Cruikshank, D.P. Dalle Ore, C.M. Clark, R.N. Pendleton, Y.J. (2014) *Aromatic and aliphatic organic materials on*
705 *Iapetus: Analysis of Cassini VIMS data*. Icarus. 233. 306-315
706 Dartnell, L.R. Patel, M.R. Storrie-Lombardi, M.C. Ward, J.M. Muller. J.P. (2012). *Experimental determination of*
707 *photostability and fluorescence-based detection of PAHs on the Martian surface*. Meteorics and Planetary Science.
708 47. 5. pp.806-819
709 Douté, S., B. Schmitt, Y. Langevin, J.-P Bibring, F. Altieri, G. Bellucci, B. Gondet, F. Poulet and the MEX OMEGA
710 Team (2007). *South pole of Mars: Nature and composition of the icy terrains from Mars Express OMEGA*
711 *observations.* Planet. Space Science, 55, 113-133.
712 Dullemond, P. Henning, T.H. Visser, R. Geers, V.C. van Dishoeck, E.F. Pontoppidan, K.M. (2007). *Dust*
713 *sedimentation in protoplanetary disks with polycyclic aromatic hydrocarbons.* Astronomy and Astrophysics. 473.
714 457-466
715 Fairén, A.G. Davila, A.F. Lim, D. Bramall, N. Bonaccorsi, R. Zavaleta, J. Uceda, E.R. Stoker, C. Wierzchos, J. Dohm,
716 J.M. Amils, R. Andersen, D. McKay, C.P. (2010). *Astrobiology through the Ages of Mars: The Study of Terrestrial*
717 *Analogues to Understand the Habitability of Mars*. Astrobiology. 10. 8. 821-843
718 Freissinet, C. Glavin, D.P Mahaffy, P. R. Miller, K. E. Eigenbrode, J. L. Summons, R. E. Brunner, A. E. Buch, A.
719 Szopa, C. Archer Jr., P. D. Franz, H. B. Atreya, S. K. Brinckerhoff, W. B. Cabane, M. Coll, P. Conrad, P. G. Des
720 Marais, D. J. Dworkin, J. P. Fairén, A. G. François, P. Grotzinger, J. P. Kashyap, S. ten Kate, I. L. Leshin, L. A.
721 Malespin, C. A. Martin, M. G. Martin. Torres, F. J. McAdam, A. C. Ming, D. W. Navarro-González, R. Pavlov, A.
722 A. Prats, B. D. Squyres, S. W. Steele, A. Stern, J. C. Sumner, D. Y. Sutter, B. Zorzano, M.-P. The MSL Science Team.
723 (2015). *Organic molecules in the Sheepbed Mudstone, Gale Crater, Mars.* Journal of Geophysical Research: Planets.
724 120. 3. 495-514.

Grisolle F. (2013*). Les condensats saisonniers de Mars : étude expérimentale de la formation et du métamorphisme de glaces de CO_2. PhD thesis*, Université Joseph Fourier, Grenoble. [TEL: https://tel.archives-ouvertes.fr/tel-01167247/document]

Herbst, E. van Dishoek, E.F. (2009). *Complex Organic Interstellar Molecules. Annual Review of Astronomy and Astrophysics.* 47. 427-480

Grundy, W.; Schmitt, B. (1997): *NIR Optical constants spectrum of H2O Ih crystal and H2O liquid from 20 to 293 K.* SSHADE/GhoSST (OSUG Data Center). Dataset/Spectral Data. https://doi.org/10.26302/SSHADE/EXPERIMENT_BS_20120924_011.

Grundy, W., and B. Schmitt 1998. *The temperature-dependent near-infrared absorption spectrum of hexagonal H_2O ice*. J. Geophys. Res. E, **103,** 25809-25822.

Hansen, G. (2005). *Ultraviolet to near-infrared absorption spectrum of carbon dioxide ice from 0.174 to 1.8 μm*. Journal of Geophysical Research, 110, E11003.

Hecht, M.H., Kounaves, S.P., Quinn, R.C., West, S.J., Young, S.M.M., Ming, D.W., Catling, D.C., Clark, B.C., Boynton, W.V., Hoffman, J. and DeFlores, L.P., (2009). *Detection of perchlorate and the soluble chemistry of Martian soil at the Phoenix lander site.* Science, 325(5936), pp.64-67

Izawa, M.R.M., Applin, D.M., Norman, L. and Cloutis, E.A., (2014). *Reflectance spectroscopy (350–2500 nm) of solid-state polycyclic aromatic hydrocarbons (PAHs).* Icarus, 237, pp.159-181.

Jian, J.J. Ip,W.H. (2009). *Seasonal patterns of condensation and sublimation cycles in the cryptic and non-cryptic regions of the South Pole*. Advances in Space Research. 43. pp.138-142

Langevin,Y., J.-P. Bibring, F. Montmessin, F. Forget, M. Vincendon, S. Douté, F. Poulet, and B. Gondet (2007). *Observations of the south seasonal cap of Mars during recession in 2004–2006 by the OMEGA visible/near-infrared imaging spectrometer on board Mars Express*. Journal of Geophysical Research, 112, E08S12.

Kalpana, M.S., Babu, E.V.S.S.K., Mani, D., Tripathi, R.P. and Bhandari, N., (2021). *Polycyclic aromatic hydrocarbons in the Mukundpura (CM2) Chondrite*. Planetary and Space Science, 198, p.105177.

Klein, H.P., (1978). *The Viking biological experiments on Mars.* Icarus, 34(3), pp.666-674

Li, A. (2008). *PAHs in comets: An overview.* Physics and Astronomy. 53. 31-44. DOI: https://doi.org/10.1007/978-3-540-76959-0_21

Lopez-Puertas, M. Dinelli, B.M. Adriani. A. Funke, B. Garcia-Comas, M. Moriconi, M.L. D'Aversa, E.D. Boersma, C. Allamandola, L.J. (2013). *Large abundances of polycyclic aromatic hydrocarbons in Titan's upper atmosphere*. The Astrophysical Journal. 770.132. 1-8

Malin, M.C. Caplinger, M.A. Davis, S.D. (2001). *Observational evidence for an active surface reservoir of solid carbon dioxide on Mars.* Science. 294. 2146-2148.

McKay D. S., Gibson E. K., Jr., Thomas-Keprta K. L., Vali H., Romanek C. S., Clemett S. J., Chillier X. D. F., Maechling C. R., and Zare R.N. (1996) *Search for past life on Mars: Possible relic biogenic activity in martian meteorite ALH84001*. Science 273, 924-930.

Mulas, G. Malloci, C. Joblin, C. Toublanc, D. (2005). *Estimated IR and phosphorescence emission fluxes for specific Polycyclic Aromatic Hydrocarbons in the Red Rectangle.* Astronomy and Astrophysics. 446. pp.537-549

762 Murchie, S. Arvidson, R. Bedini, P. Beisser, K. Bibring, J-P. Bishop, J. Boldt, J. Cavender, P. Choo, T. Clancy, R.T.
763 Darlington, E.H. Des Marais, D. Espiritu, R. Fort, D. Green, R. Guinness, E. Hayes, J. Hash, C. Heffernan, K.
764 Hemmler, J. Heyler, G. Humm, D. Hutcheson, J. Izenberg, N. Lee, R. Lees, J. Lohr, D. Malaret, E. Martin, T.
765 McGovern, J.A. McGuire, P. Morris, P. Mustard, J. Pelkey, S. Rhodes, E. Robinson, M. Roush, T. Schaefer, E.
766 Seagrave, G. Seelos, F. Silverglate, P. Slavney, S. Smith, M. Shyong, W.J. Strohbehn, K. Taylor, H. Thompson, P.
767 Tossman, B. Wirzburger, M. Wolff, M. (2007). *Compact Reconnaissance Imaging Spectrometer for Mars (CRISM)*
768 *on Mars Reconnaissance Orbiter (MRO).* Journal of Geophysical Research. 112. E05S03, doi:10.1029/2006JE002682
769 Navarro-González, R., Vargas, E., de La Rosa, J., Raga, A.C. and McKay, C.P., (2010). *Reanalysis of the Viking*
770 *results suggests perchlorate and organics at midlatitudes on Mars.* Journal of Geophysical Research: Planets,
771 115(E12)
772 Oberg, K.I. Garrod, R.T. van Dishoek, E.F. Linnartz, H. (2009). *Formation rates of complex organics in UV irradiated*
773 *CH_3OH-rich ices*. Astronomy and Astrophysics. 504. 3. 891-913
774 Ojha, L. Willhelm, M.B. Murchie,. S.L. MEwen, S.S. Wray, J.J. Hanley, J. Masse. M. Chojnacki, M. (2015). *Spectral*
775 *evidence for hydrated salts in recurring slope lineae on Mars*. Nature Geoscience. 8. 829-832.
776 Orosei, R. Lauro, S.E. Pettinelli, E. Cicchetti, A. Coradini, M. Cosciotti, B. Di Paulo, F. Flamini, E. Mettei, E.
777 Pajola, M. Soldovieri, F. Cartacci, M. Cassenti, F. Frigeri, A. Giuppi, S. Martufi, R. Masdea, A. Mitri, A. Nenna, C.
778 Noschese, R. Restano, M. Seu, R. (2018). *Radar evidence of subglacial liquid water on Mars*. Science. DOI:
779 10.1126/science.aar7268
780 Philippe S. (2016). *Microphysique des processus saisonniers des glaces de Mars et Pluton : suivi par télédétection*
781 *hyperspectrale et étude expérimentale*. *PhD thesis*, Université Grenoble Alpes, Grenoble. [TEL: https://tel.archives-
782 ouvertes.fr/tel-01560378/document]
783 Piquex.S. Edwards, C.S. Christensen, P.R. (2008). *Distribution of the ices exposed near the south pole of Mars using*
784 *THEMIS temperature measurements*. Journal of Geophysical Research. 113. E02006
785 Plaxco, K.W. Gross, M. (2011). *Astrobiology: A Brief Introduction*. 2nd Edition. The John Hopkins University Press.
786 pp.145-152
787 Quirico, Eric; Schmitt, Bernard (2004): *Near-IR optical constants of crystalline CO_2 ice at 179 K completed with 28K*
788 *data*. SSHADE/GhoSST (OSUG Data Center). Dataset/Spectral Data.
789 https://doi.org/10.26302/SSHADE/EXPERIMENT_BS_20130215_001
790 Sandford, S. A., M. P. Bernstein, and C. K. Materese (2013). *The infrared spectra of polycyclic aromatic hydrocarbons*
791 *with excess peripheral H atoms (Hn-PAHs) and their relation to the 3.4 and 6.9μm PAH emission features*. The
792 Astrophysical Journal Supplement Series, 205:8.
793 Schuerger, A.C and Clark, B.C., (2008). *Viking biology experiments; Lessons learned and the role of ecology in future*
794 *life-detection experiments.* In Strategies of Life Detection (pp. 233-243_. Springer, Boston, MA
795 Smith, M.D., (2004). *Interannual variability in TES atmospheric observations of Mars during 1999–*
796 *2003*. Icarus, 167(1), pp.148-165.
797 Tang N. (2018) PAHs/NPAHs. In: Hayakawa K. (eds) *Polycyclic Aromatic Hydrocarbons*. Springer, Singapore.
798 https://doi.org/10.1007/978-981-10-6775-4_3

799 Thompson, M.S., Morris, R.V., Clemett, S.J., Loeffler, M.J., Trang, D., Keller, L.P., Christoffersen, R. and Agresti,
800 D.G., (2020). *The effect of progressive space weathering on the organic and inorganic components of a*
801 *carbonaceous chondrite*. Icarus, 346, p.113775.
802 Vincent, W.F. Rae, R. Laurion, I. Howard-Willimans, C. Priscu, J.C. (1998). *Transparency of Antarctic ice-covered*
803 *lakes to solar UV radiation.* Limnology and Oceanography. 43. 4. 618-624
804 Wright, I.P., Grady, M.M. and Pillinger, C.T., (1989). *Organic materials in a Martian meteorite*. Nature, 340(6230),
805 pp.220-222.